




# Precision transcriptomics of viral foci reveals the spatial regulation of immune-signaling genes and identifies *RBOHD* as an important player in the incompatible interaction between potato virus Y and potato

Tjaša Lukan<sup>1,\*</sup> , Maruša Pompe-Novak<sup>1,†</sup>, Špela Baebler<sup>1,†</sup> , Magda Tušek-Žnidarič<sup>1</sup> , Aleš Kladnik<sup>2</sup> , Maja Kriznik<sup>1</sup>, Andrej Blejec<sup>1</sup> , Maja Zagorščak<sup>1</sup> , Katja Stare<sup>1</sup> , Barbara Dušak<sup>1</sup> , Anna Coll<sup>1</sup> , Stephan Pollmann<sup>3</sup> , Karolina Morgiewicz<sup>4</sup>, Jacek Hennig<sup>4</sup> , and Kristina Gruden<sup>1</sup> 

<sup>1</sup>National Institute of Biology, Večna pot 111, Ljubljana 1000, Slovenia,

<sup>2</sup>Biotechnical Faculty, University of Ljubljana, Jamnikarjeva 101, Ljubljana 1000, Slovenia,

<sup>3</sup>Centre for Plant Biotechnology and Genomics, Campus de Montegancedo, Crta M-40, Km 38, Pozuelo de Alarcón, Madrid 28223, UPM-INIA Spain, and

<sup>4</sup>Institute of Biochemistry and Biophysics, Polish Academy of Sciences, Pawińskiego 5a, Warsaw 02-106, Poland

Received 29 March 2020; accepted 21 July 2020; published online 9 August 2020.

\*For correspondence (e-mail tjas.lukan@nib.si).

†Shared first authorship.

## SUMMARY

Whereas the activation of resistance (R) proteins has been intensively studied, the downstream signaling mechanisms leading to the restriction of the pathogen remain mostly unknown. We studied the immunity network response conditioned by the potato *Ny-1* gene against potato virus Y. We analyzed the processes in the cell death zone and surrounding tissue on the biochemical and gene expression levels in order to reveal the spatiotemporal regulation of the immune response. We show that the transcriptional response in the cell death zone and surrounding tissue is dependent on salicylic acid (SA). For some genes the spatiotemporal regulation is completely lost in the SA-deficient line, whereas other genes show a different response, indicating multiple connections between hormonal signaling modules. The induction of NADPH oxidase *RBOHD* expression occurs specifically on the lesion border during the resistance response. In plants with silenced *RBOHD*, the functionality of the resistance response is perturbed and the spread of the virus is not arrested at the site of infection. *RBOHD* is required for the spatial accumulation of SA, and conversely *RBOHD* is under the transcriptional regulation of SA. Using spatially resolved RNA-seq, we also identified spatial regulation of an UDP-glucosyltransferase, another component in feedback activation of SA biosynthesis, thus deciphering a novel aspect of resistance signaling.

**Keywords:** immune signaling network, NADPH oxidase *RBOHD*, reactive oxygen species, salicylic acid, *Solanum tuberosum* (potato), spatiotemporal response analysis, virus resistance, *Potyvirus*.

## INTRODUCTION

Plants have evolved sophisticated mechanisms to perceive pathogen attack and effectively respond. Besides passive defenses, plants possess a multilayered actively induced immune system. The first most general layer, pathogen-associated molecular-pattern-triggered immunity (PTI), is based on the recognition of pathogen components, common for a number of pathogens, by the plant pattern recognition receptors. The more specific layers of immunity are mediated by intracellular resistance (R) proteins (Jones and Dangl, 2006). R proteins confer the recognition

of pathogen-derived effectors and initiate effector-triggered immunity (ETI). One of the manifestations of a successful immune response is hypersensitive response (HR)-conferred resistance, where restriction of pathogens to the infection site is associated with a form of localized programmed cell death (PCD) (Künstler *et al.*, 2016). HR-conferred resistance is preceded by a series of biochemical and cellular signals. One of the earliest hallmarks of HR is the rapid and intense production of reactive oxygen species (ROS) (Balint-Kurti Peter, 2019). Salicylic acid (SA) is required for the restriction of pathogens during HR in various pathosystems, including viruses (Mur *et al.*, 2008;

Künstler *et al.*, 2016; Calil and Fontes, 2017) such as tobacco mosaic virus (TMV) (Chivasa *et al.*, 1997; Chivasa and Carr, 1998) and potato virus Y (PVY) (Baebler *et al.*, 2014; Lukan *et al.*, 2018). The effectiveness of downstream events in ETI is also regulated by jasmonic acid (JA) and ethylene (ET) (Baebler *et al.*, 2014). The PTI layer of immunity arising from plant–virus interaction is much less understood. It has been shown only recently that double-stranded RNA (dsRNA) is a viral pathogen-associated molecular pattern (PAMP) that triggers a signaling cascade similar to the PTI in other pathosystems (Niehl *et al.*, 2016). Other hormones have also been shown to play important roles in plant immunity (Pieterse *et al.*, 2012; Li *et al.*, 2019). The activation of the immune signaling network results in the induced expression of effectors of defense, such as pathogenesis-related protein 1 (PR-1) and beta-glucosidases, yet their function is not fully understood (Morant *et al.*, 2008; Breen *et al.*, 2017). HR-associated PCD was shown to restrict pathogen spread in some (hemi)biotrophic pathosystems (Dickman and de Figueiredo, 2013; Lee *et al.*, 2015b). It has been shown that it is not required for resistance in several viral pathosystems (reviewed in Künstler *et al.*, 2016), however, including the potato–PVY interaction (Lukan *et al.*, 2018).

Precise temporal and spatial coordination of induced signaling pathways is required to successfully restrict the pathogen with minimal damage to the host (reviewed in Künstler *et al.*, 2016). The concentric spread, typical of many viruses, results in foci containing cells at different stages of infection (Yang *et al.*, 2007; Rupar *et al.*, 2015). The immune response signal is, however, transferred to the surrounding tissue, resulting in a gradient of response in the surrounding cells (Dorey *et al.*, 1997; Havelda and Maule, 2000; Maule *et al.*, 2002; Yang *et al.*, 2007).

Potato virus Y (PVY), a member of the genus *Potyvirus* from the family Potyviridae, is the most harmful virus of cultivated potatoes (Karasev and Gray, 2013) and is among the most economically important viruses infecting plants (Quenouille *et al.*, 2013). The most studied type of resistance to PVY is HR-conferred resistance (Karasev and Gray, 2013). In potato cv. Rywal, HR is initiated by the *Ny-1* gene and manifests as the formation of necrotic lesions on inoculated leaves (Szajko *et al.*, 2008). We have shown previously that the transcriptional dynamics of genes known to participate in the immune response is crucial for the efficient resistance response and that SA is the key component in the orchestration of these events (Baebler *et al.*, 2014).

In order to dissect the mechanisms acting downstream of the activation of the *Ny-1* R protein in the resistance response, we analyzed the processes at work on the biochemical, ultrastructural and gene expression levels in the cell death zone and surrounding tissue in a spatiotemporal manner. To evaluate the position of SA in the signaling

cascade, we analyzed in parallel the responses of SA-depleted NahG plants.

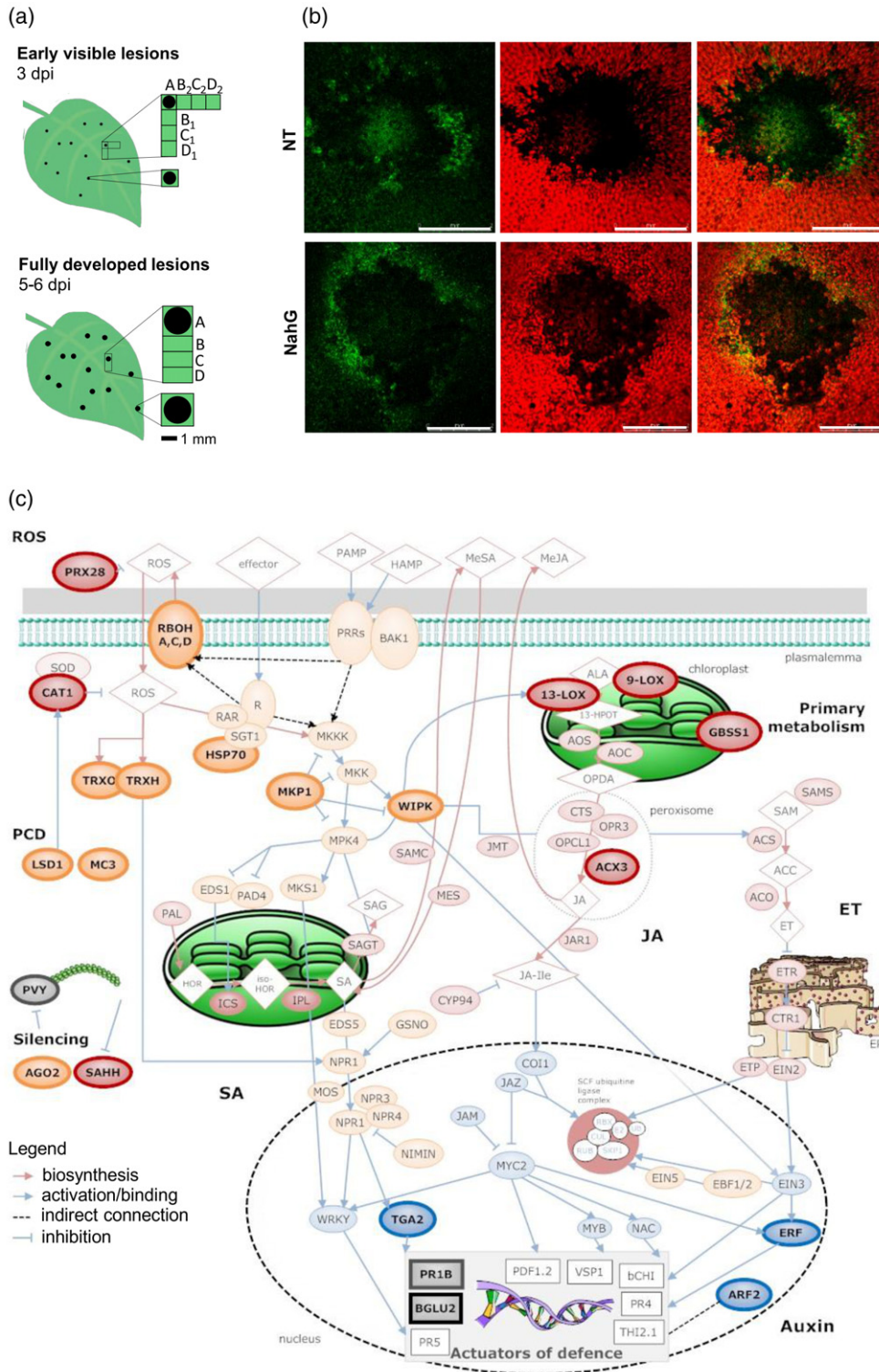
## RESULTS

### The transcriptional response of immune signaling-related genes is diversely spatially regulated

Previously, we performed a non-targeted transcriptional analysis of inoculated homogenized leaves at 1, 3 and 6 days post-inoculation (dpi) in potato cv. Rywal leaves infected with PVY (Baebler *et al.*, 2014). The results of our several independent experiments showed that responses can vary between plants, which is also related to the number of lesions formed on the leaves. We thus hypothesized that a more detailed spatial analysis of responses would provide better insights into the processes involved in the resistance response downstream of *Ny-1* activation. In response to PVY<sup>N-Wilga</sup>, the phenotypes of potato (cv. Rywal, hereafter NT) and a transgenic counterpart, depleted in the accumulation of SA (NahG-Rywal, hereafter NahG, with SA reduced to <10% of native values; Baebler *et al.*, 2014), were as previously described (Baebler *et al.*, 2014; Lukan *et al.*, 2018; Figure S1). Although resistance was successful in NT and the virus was restricted to the inoculated leaves, the depletion of SA rendered NahG plants susceptible (catechol independent; Baebler *et al.*, 2014), allowing the virus to spread throughout the plant accompanied by the development of lesions (Figure S1).

We developed a protocol for the precise sampling of tissue sections surrounding the lesion at different stages of lesion development (early visible lesions at 3 dpi and fully developed lesions at 5–6 dpi; Figure 1a), suitable for transcriptomics and hormonomics analyses. As the quantities of RNA obtained from individual small tissue sections (approximately 400 cells; Figure S2) are limited, we first selected 23 genes from our microarray data set according to their biological function and responsiveness (Baebler *et al.*, 2014; Table S1), including genes participating in redox potential homeostasis (*CAT1*, *PRX28*, *RBOHD*, *RBOHA*, *RBOHC*, *TRXO* and *TRXH*), cell death (*MC3* and *LSD1*), RNA silencing (*AGO2* and *SAHH*), MAP kinase cascade (*WIPK* and *MKP1*), SA (*TGA2*), JA (*13-LOX*, *9-LOX*, *ACX3*), ET (*ERF1*) or auxin (*ARF2*) signaling, effectors of defense (*BGLU* and *PR1B*) or a marker for starch metabolism (*GBSSI*) (Figure 1c). In parallel with the gene expression of those genes, the relative quantity of PVY RNA was measured by quantitative PCR (qPCR; Data S1 and S2).

First, we analyzed fully developed lesions that developed 5–6 days following inoculation with PVY<sup>N-Wilga</sup> (Figure 1a). The highest quantity of viral RNA was found in the center of the lesion in both potato genotypes, but the expression pattern of the genes changed with distance from the center of the lesion, and in some cases the response differed between the two genotypes (Figure 2). The response did



not differ if the plant was inoculated with different viral strains, however (PVY<sup>NTN</sup> and PVY<sup>N-GFP</sup>; Figure S3). As the lesion diameter is somewhat larger in NahG plants at the stage when we collected the fully developed lesions

(up to twofold larger in NahG compared with NT plants; Figure S2; Data S3), note that some of the response measured in section B of the fully developed lesions of NahG plants is captured within section A in NT plants. We

**Figure 1.** Experimental set-up.

(a) Sections containing lesion (section A) and surrounding tissues (sections B, C and D, consecutive 1-mm strips distal to section A) were sampled at two different time points. Tissue surrounding early visible lesions was sampled in two perpendicular directions, here marked with 1 and 2, respectively. For electron microscopy, tissue sections with a lesion and surrounding cells were sampled. In mock-inoculated plants, four adjacent tissue sections of the same size as used in inoculated leaves were excised from different plants. Scale bar: 1 mm.

(b) PVY<sup>N</sup>-GFP accumulation around fully developed lesions in non-transgenic (NT, top) or in SA-depleted (NahG, bottom) plants. From left to right: PVY<sup>N</sup>-GFP accumulation (green), chlorophyll fluorescence (red), overlay of chlorophyll fluorescence and PVY<sup>N</sup>-GFP accumulation. Scale bar: 2 mm.

(c) Plant immune signaling-related genes selected for the initial transcriptomic spatiotemporal response analysis. Potato virus Y (PVY) accumulation and expression of genes involved in reactive oxygen species (ROS), MAP kinase signaling, programmed cell death (PCD), salicylic acid (SA), jasmonic acid (JA), ethylene (ET), auxin and starch metabolism were analyzed (bold border). Signaling proteins are presented as orange, enzymes as red and transcription factors as blue ovals, respectively; metabolites are presented as diamonds and genes as squares. *ACX3*, acyl-CoA oxidase; *AGO2*, argonaute 2; *ARF2*, auxin response factor 2; *BGLU2*, 1,3-β-glucosidase; *CAT1*, catalase 1; *ERF1*, potato ethylene responsive transcription factor 1a; *GBSS1*, granule-bound starch synthase 1; *HSP70*, heat shock protein 70; *9-LOX*, 9-lipoxygenase; *13-LOX*, 13-lipoxygenase; *LSD1*, zinc-finger protein LSD1; *MC3*, metacaspase 3; *MKP1*, mitogen-activated protein kinase phosphatase 1; *PR1B*, pathogenesis-related protein 1b; *PRX28*, peroxidase 28; *RBOHA*, potato respiratory burst oxidase homolog A; *RBOHC*, potato respiratory burst oxidase homolog C; *RBOHD*, potato respiratory burst oxidase homolog D; *SAHH*, adenosylhomocysteinase S-adenosyl-L-homocysteine hydrolase; *TGA2*, bZIP transcription factor family protein; *TRXH*, thioredoxin H; *TRXO*, thioredoxin O; *WIPK*, potato wound-inducible protein kinase. For gene IDs and primer information, see Table S3.

collected the samples as soon as the dark lesion was visible in order to minimize this effect. Such early sampling was also necessary to only follow the effect of the depletion of SA and not also the multiplication of PVY (Figures S2 and S3). The expression of *HSP70* (see Figure 1c for full gene names), encoding a protein involved in the stability of R proteins (Kadota and Shirasu, 2012), is elevated in the center of viral foci (section A) compared with the adjacent sections (sections B, C and D) only in non-transgenic (NT) plants (Figure 2). Both *BGLU2* and *PR1B* are also under the regulation of SA (Figure 2). Although these genes do indeed show strong upregulation close to the center of viral infection (more than 10-fold compared with the distal tissue, section D) during the resistance response, this response differs markedly in the SA-depleted system. Whereas the spatial response of *BGLU2* in NahG plants is completely lost, the peak of the *PR1B* response occurs further away from the foci of viral infection (reaching a peak in section C; Figure 2). The regulation of *ERF1*, involved in ET signaling, resembles that of *PR1B* in both genotypes. The spatial profile of starch synthase *GBSS1*, an indicator of primary metabolism state, shows that starch metabolism is downregulated in the center of the lesion, and its proximity, whereas in section D its expression status is closer to that of the mock-inoculated leaf tissue (Figure 2, denoted with empty circles at the end of the x-axis). This is not true in NahG plants, however, where the expression of *GBSS1* is downregulated even further away from the lesion (Figure 2).

We also show that the expression of genes involved in JA biosynthesis, in the maintenance of redox potential and in cell death is spatiotemporally regulated, which is presented in more detail in the next sections. For some genes the transcriptional response in the cell death zone and surrounding tissue depends upon SA, with a lack of SA leading either to no response (for *BGLU2*, *ACX3*, *RBOHA*, *RBOHD*, *TRXH* and *GBSS1*) or to a changed spatiotemporal profile of the response (for *ERF1*, *PR1B*, *CAT1* and *PRX28*) (Figures S4 and S5; Data S1). The rest of the genes analyzed are not SA-dependent, showing either no spatial

regulation at all or responding in an asynchronous manner between biological replicates (*ARF2*, *RBOHC*, *13-LOX*, *WIPK*, *MKP1*, *AGO2*, *SAHH*, *LSD1*, *MC3*, *9-LOX*, *HSP70* and *TGA2*); Figures S4 and S5; Data S1), meaning that most probably their regulation is even more finely tuned and that more detailed analysis (e.g. with single-cell resolution) would be required.

Next, we wanted to implement our approach in the earlier stages of viral infection. As the first robust time point for spatial analysis of responses, we identified the early visible lesions that develop at 3 dpi. These lesions are visible only when leaves are transilluminated (Figure 1a). Indeed, when comparing the response profiles of different lesions and profiles within the same lesion in perpendicular directions, the results were consistent and enabled a reliable biological interpretation (Figures S6 and S7; Data S2). Comparison of spatial response profiles in both time points enabled the identification of unexpected regulation. For example, the JA signaling module is not uniformly spatiotemporally regulated. The *13-LOX* gene, encoding 13 lipoxygenases at the start of the oxylipin branch, leading to JA biosynthesis, is induced in the center of viral foci at the stage of fully developed lesions (Figure S8). In agreement with the hypothesis that JA and SA are antagonistic, the response is enhanced in NahG plants. The expression pattern of the *ACX3* gene, involved in later steps of JA biosynthesis (Figure 1c), is regulated similarly, except for the diminished regulation at the stage of fully developed lesions of NahG plants (Figure S8). This shows that besides JA signaling, SA signaling is also required for the spatiotemporal response of the *ACX3* gene. Our results thus indicate that as yet unknown connections between different components of immunity signaling exist.

### The ultrastructural features in the cell death zone and surrounding tissue are not dependent on SA

Our next hypothesis was that SA depletion influences processes that lead to changes in ultrastructural features in and surrounding the site of viral entry, thus rendering the

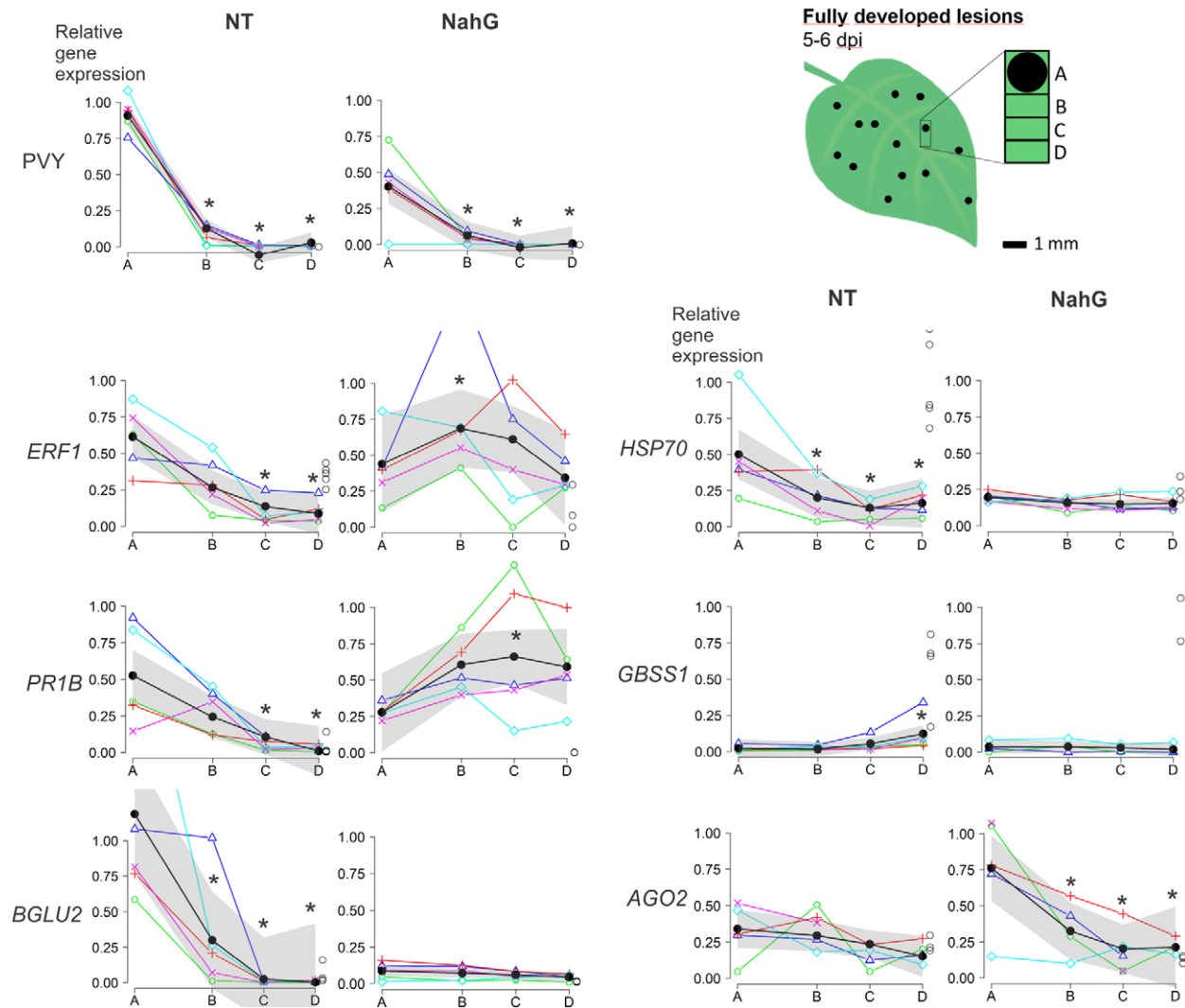


**Figure 2.** The lack of SA leads to the diverse spatial transcriptional regulation of immune-related genes.

Transcriptional profiles of the selected genes were monitored in non-transgenic (NT) and SA-depleted (NahG) plants following inoculation with PVY<sup>N-Wilga</sup> at the stage of fully developed lesions (5–6 dpi). Distance from the lesion center, marked as positions A, B, C and D, is plotted on the x-axis and relative gene expression is plotted on the y-axis. Expression values in mock-inoculated tissue sections are shown as empty circles at the end of x-axis. Asterisks denote the statistical significance ( $P < 0.05$ ) of gene expression at positions B, C and D, compared with that at position A. Spatial profile models are shown as thick black lines, with 95% confidence interval bands presented in gray. Relative gene expression values within individual lesions are presented with colored symbols connected by a line. Full gene names are given in the legend of Figure 1.

immune response ineffective. In the center of lesions the cells were in the final stages of the cell death process, and only the cell wall and a small volume of electron-dense material were visible (Figure S9). The transition between these and normal cells was limited to a narrow layer of cells of different types (Figure 3), both at the stage of early and fully developed lesions. In parenchymal and bundle sheath cells cytoplasmic vacuolization, an autophagy feature, was in progress (Figure 3a,c,f). Many chloroplasts were deformed or degraded (Figure 3b,f). No differences were observed between both the genotypes studied (Figure 3), however, indicating that the features of the

processes observable at this level (PCD, autophagy, ER stress, etc.) do not depend on SA.

### The expression of genes involved in redox-state maintenance is tightly regulated across the spatiotemporal scale studied

We next focused our research on genes involved in the generation and quenching of ROS as redox potential changes are one of the first responses to pathogen recognition, both in PTI and ETI (Figure 1c). We studied three *RBOH* genes involved in the generation of apoplastic ROS and leading to redox changes in the cytoplasm. On the quenching side, we

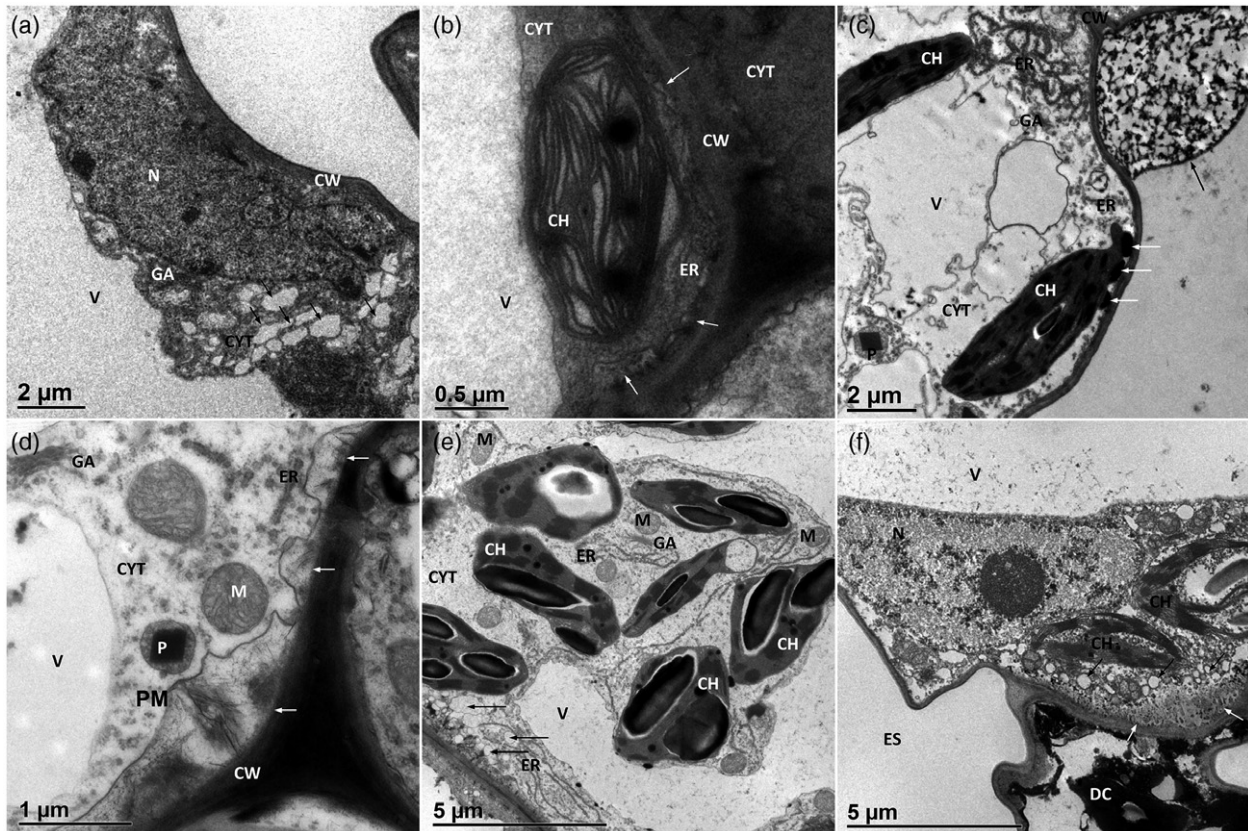


**Figure 3.** Ultrastructural features of the hypersensitive response are not dependent on salicylic acid. The same features were observed at the border of the cell death zone in both non-transgenic (a–c) and NahG plants (d–f).

- (a) Ameboidal nucleus and vacuolized cytoplasm in bundle sheath cell.  
 (b) Electron-dense cytoplasm, disorganized thylakoid (distortion of grana with larger interthylakoidal spaces) in chloroplast and detachment of plasmalemma from the cell wall (white arrows) of the companion cell.  
 (c) Highly vacuolated cytoplasm and accumulation of electron-dense material inside (white arrows) and outside (black arrow) the cell.  
 (d) Detachment of plasmalemma from the cell wall (white arrows) in bundle sheath cell.  
 (e) Degradation of chloroplasts and increased endoplasmic reticulum in mesophyll cell.  
 (f) Detachment of plasmalemma (white arrows), vacuolization of cytoplasm (black arrows), beginning of chromatin condensation and degradation of chloroplasts in bundle sheath cell. CH, chloroplast; CW, cell wall; CYT, cytoplasm; DC, destroyed cell; ER, endoplasmic reticulum; ES, extracellular space; GA, Golgi apparatus; M, mitochondrion; N, nucleus; P, peroxisome; PM, plasmalemma; V, vacuole.

analyzed gene expression of *CAT1*, located in the peroxisome, and apoplastic peroxidase *PRX28*. Additionally, we monitored the gene expression of two cytoplasmic redox potential sensor proteins that were implicated in the regulation of immune signaling, thioredoxins H and O (*TRXH* and *TRXO*). The three *RBOH* genes investigated each demonstrate distinct spatiotemporal regulation. *RBOHC* is not regulated in any of the genotypes studied (Figure 4). *RBOHA* is strongly induced in the center of viral foci already in the early stage of lesion development, whereas this activation is attenuated in NahG plants. *RBOHD*, however, responds in section A in the early stages, whereas later on it forms a peak of expression close to the border of the lesion itself in the majority of lesions (Figure 4). *RBOHD* is also under the regulation of SA as this gene is expressed close to the limit of quantification in NahG plants. *PRX28* is induced earlier in NahG plants, and at the stage of fully developed lesion its

expression peaks in section A in NT plants and in section B in NahG plants. *CAT1* is induced only in NahG plants and is induced even further away from the center of viral foci compared with *PRX28*. At the stage of early lesions it peaks in section C, and at the stage of fully developed lesions it peaks even further from the center of the lesion, in section D. The expression of *TRXO* was below the limit of quantification, and therefore it was not possible to follow its response. Interestingly, however, *TRXH* responds strongly and early only in NT plants.

We further wanted to inspect how changes in transcriptional activity of ROS-related genes are reflected in the accumulation of  $H_2O_2$ . We followed  $H_2O_2$  production in relation to lesion size at several time points following virus inoculation. In contrast to the visible lesion growth pattern (Figure 5a), the  $H_2O_2$  accumulation area around the lesions was significantly larger in NahG plants after 5 dpi

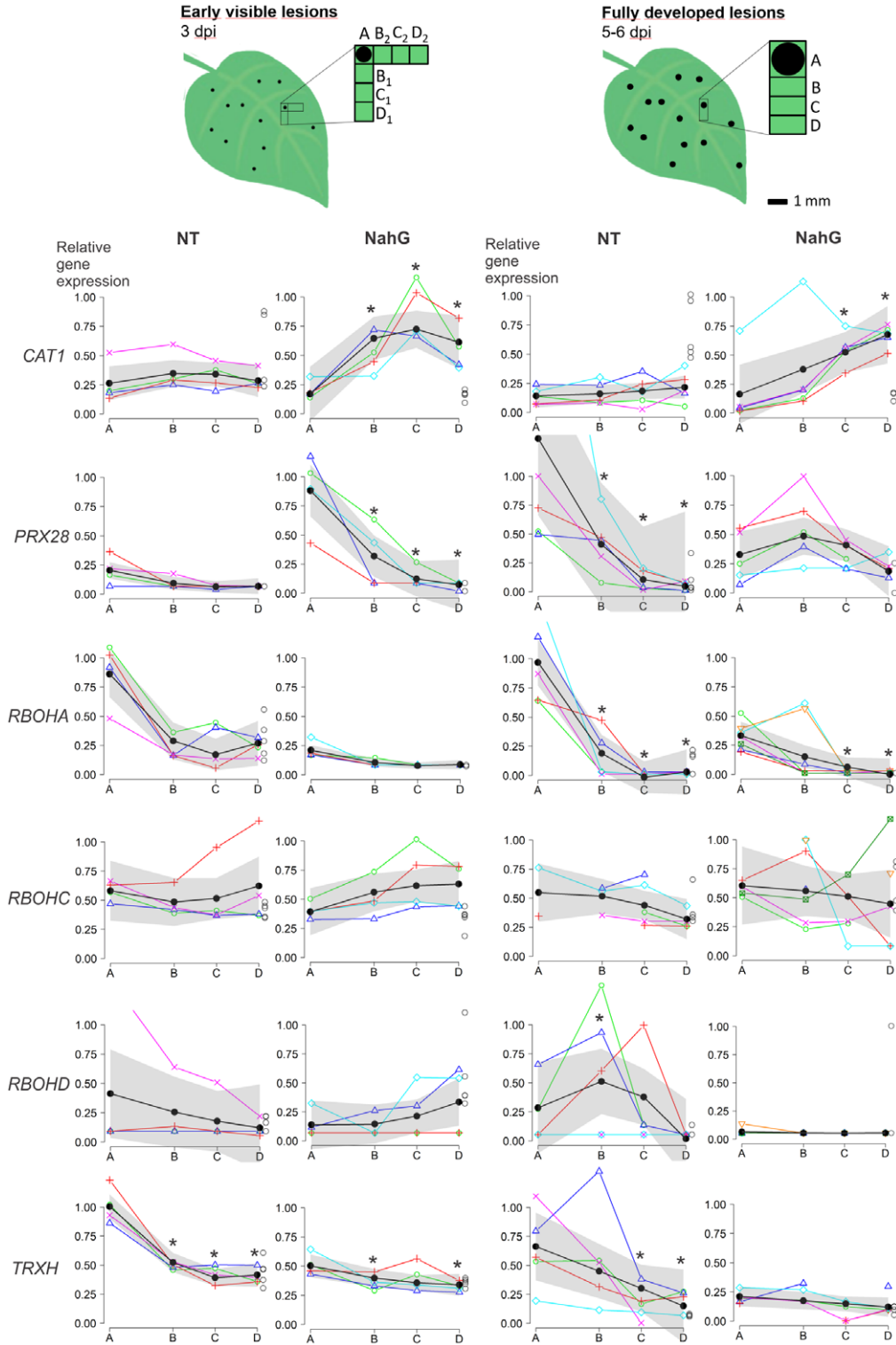


**Figure 4.** The induction of expression of *RBOHD* is limited to the cells immediately surrounding the infected tissue. Spatial expression profiles of selected genes for non-transgenic (NT) and SA-depleted (NahG) plants after inoculation with potato virus Y at the stage of early visible lesions (3 dpi, left, averaged profile of the two perpendicular directions) and fully developed lesions (5–6 dpi, right). For the full gene names and full description of the graphs, see the legends to Figures 1 and 2, respectively.

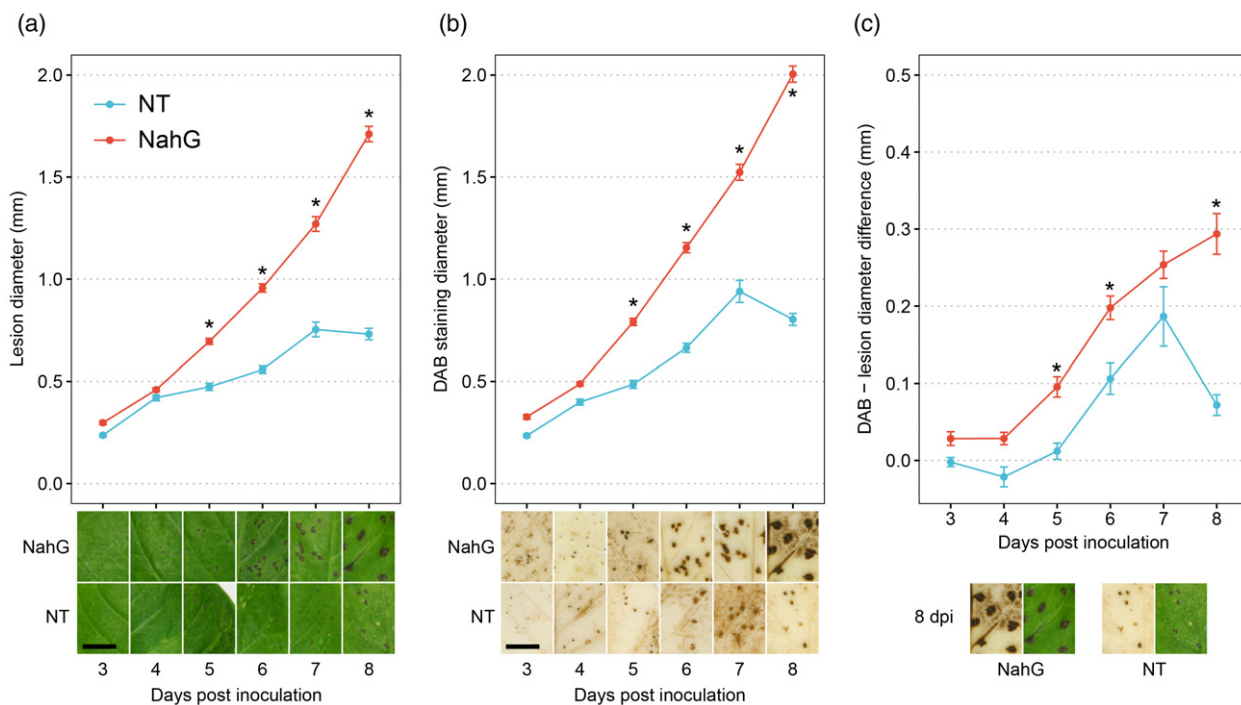


**Figure 5.** H<sub>2</sub>O<sub>2</sub> accumulation is continuously greater during infection with potato virus Y in potato plants perturbed in SA signaling.

(a) Lesion diameter was significantly larger in the NahG plants from 5 dpi on compared with non-transgenic (NT) plants.

(b) DAB staining indicating H<sub>2</sub>O<sub>2</sub> activity (visible as the brown precipitate) was significantly wider in NahG plants from 5 dpi onwards, compared with NT plants.

(c) Difference in diameter of DAB staining and the diameter of the corresponding lesion, showing that in NahG plants the H<sub>2</sub>O<sub>2</sub>-positive area outside the lesion is wider in comparison with NT plants. The representative areas of leaf images and comparison of lesions and DAB staining at 8 dpi are shown under the plots (scale bar: 10 mm). Asterisks represent statistically significant differences between the two genotypes on the same day ( $P < 0.05$ ). Error bars represent standard errors.

(Figure 5b). Interestingly, the stained area continuously increased in NahG plants, whereas it reached a plateau in NT plants, indicating that ROS production is limited around the lesions in plants exhibiting resistance, but not in SA-depleted plants (Figure 5c).

#### Functional *RBOHD* contributes to the blocking of systemic PVY spread

*RBOHD* showed a specific spatiotemporal expression profile, peaking at the border of the virus amplification zone (Figure 4). To validate the involvement of ROS signaling and specifically the *RBOHD* gene in virus restriction, we constructed transgenic plants of cv. Rywal with silenced *RBOHD* gene (sh*RBOHD*; Figure S10a). We inoculated two independent transgenic lines of sh*RBOHD* (lines 13 and 14) with PVY<sup>N-GFP</sup> as the least virulent PVY strain among those used in this study (Lacomme *et al.*, 2017). *RBOHD* is, in selected transgenic lines, silenced to approximately 50% of its native transcriptional activity (Figure 6b). The virus spread systemically and lesions appeared in upper non-inoculated leaves (Figures 6a and S10c,d). The time of first lesion appearance in upper non-inoculated leaves was comparable with the time of first lesion appearance in

NahG plants, but the viral RNA quantities were lower than those found in NahG plants (Figure S10c,d). Fully functional *RBOHD* thus contributes to the long-distance movement of the virus.

We also checked whether the virus can multiply to a larger extent in the inoculated leaves of sh*RBOHD* plants by detecting viral RNA abundance and by counting the number of infection sites. The viral abundance negatively correlated ( $r = -0.85$ ) with *RBOHD* expression, taking into account all of the genotypes analyzed (Figures 6b,c, S10b,c and S11a). Next, we followed the number of lesions appearing on the inoculated leaves of the *RBOHD*-silenced transgenic lines after inoculation with PVY to study whether the reduction of *RBOHD* expression results in a higher number of PVY infection sites. We confirmed this hypothesis as the number of PVY foci on inoculated leaves of sh*RBOHD* plants was higher compared with NT plants (Figures 6d and S11b–d; Data S4). Therefore, we concluded that the virus can infect cells more easily in sh*RBOHD* plants and that it also multiplies to a larger extent in the inoculated leaves of these plants. Fully functional *RBOHD* thus contributes to blocking the initiation of viral infection, the local multiplication of the virus and the long-distance movement of the virus.



### RBOHD is involved in the tight spatial regulation of SA accumulation during the resistance response

The ROS were shown to be involved both upstream and downstream of SA signaling (Herrera-Vasquez *et al.*, 2015). To determine whether RBOHD-generated ROS are involved in the regulation of SA signaling in the resistance response, we analyzed SA induction in *shRBOHD* plants. In the pool of lesions (section A), SA was induced to the same extent as in RBOHD-silenced plants (approximately 10-fold compared with mock samples; Figure 7a; Data S5), whereas in the surrounding cells (section B) the accumulation was lower in non-transgenic plants but not in RBOHD-silenced plants. As the concentration of SA in lesions on transgenic plants did not differ significantly from the concentration in lesions on non-transgenic plants (Figure 7a), we conclude that RBOHD-generated ROS are not involved in the induction of SA biosynthesis in potato-PVY interaction. The tight spatial regulation of SA biosynthesis was lost in *shRBOHD* plants, however. Additionally, we know that *RBOHD* gene activity is under the regulation of SA as the expression of this gene is much lower in NahG plants after virus inoculation (Figures 6b and S10b; Data S1).

We have further explored the mechanisms underlying spatial regulation of SA accumulation on the border of the lesion. We performed RNA-seq analysis of the tissue within the lesion (section A) and the adjacent tissue (section B) at the time of early visible lesions for all three genotypes: NT, NahG and *shRBOHD*. This analysis provided insights into processes regulated by SA or RBOHD (Figures 8 and S12; Data S6). The majority of processes that are differentially regulated between sections A and B overlap between NahG plants and *shRBOHD* plants (Figure 8). This was expected, as the expression of RBOHD is repressed in NahG plants (Figure 6b). We also demonstrate that some of the genes and even processes/protein groups are specifically regulated only when the *RBOHD* gene is silenced, however. Most notable is the regulation of MYB transcription factors (three regulated only in the absence of *RBOHD*, and not in NT or NahG transgenic plants; Data S6) and the regulation of protein degradation (the specific regulation of several proteases as well as ubiquitin SCF and RING E3 ligases; Data S6). This shows that RBOHD has some additional roles that are independent of SA.

We further inspected the RNA-seq results for any evidence of a feedback loop indicating the role of *RBOHD* in the spatial regulation of SA accumulation. We have identified a UDP-glucosyltransferase (*UGT76D1*, Sotub10g024000) that is strongly spatially deregulated in RBOHD-silenced plants and could be directly involved in the process (Figures 7b and S13). In line with the evidence that *RBOHD* is repressed in NahG plants, a similar expression pattern is also observed in these plants. In

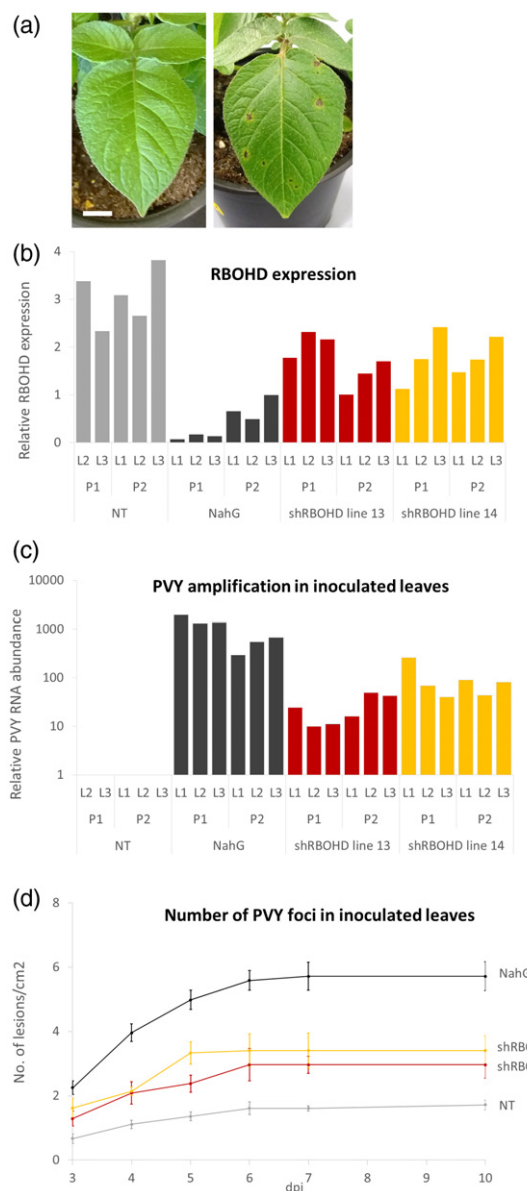


**Figure 6.** The virus efficiently multiplies in *RBOHD*-silenced plants. (a) Lesions on an upper non-inoculated leaf of *RBOHD*-silenced plant of transgenic line 14 (right) and non-transgenic counterpart (left) at 17 dpi. Scale bar: 1 cm. (b) Relative *RBOHD* expression in inoculated leaves at 6 dpi. (c) Relative potato virus Y (PVY) RNA abundance (relative to the lowest detected viral level, shown on a logarithmic scale) at 6 dpi in NT, NahG and *shRBOHD* plants. P, plant number; L, leaf number. (d) Number of lesions per cm<sup>2</sup> as they appeared on the youngest inoculated leaves of plants ( $n = 6-10$ ) of different genotypes at a particular dpi. Error bars represent the standard errors of the number of lesions per cm<sup>2</sup>. Individual measurements are available in Data S4.

Arabidopsis, *UGT76D1* is implied in the feedback activation loop of SA biosynthesis (Huang *et al.*, 2018). Overexpression of this gene led to the accumulation of SA. Here, we similarly show that the silencing of *RBOHD* results in the induction of the *UGT76D1* gene in section B, which may

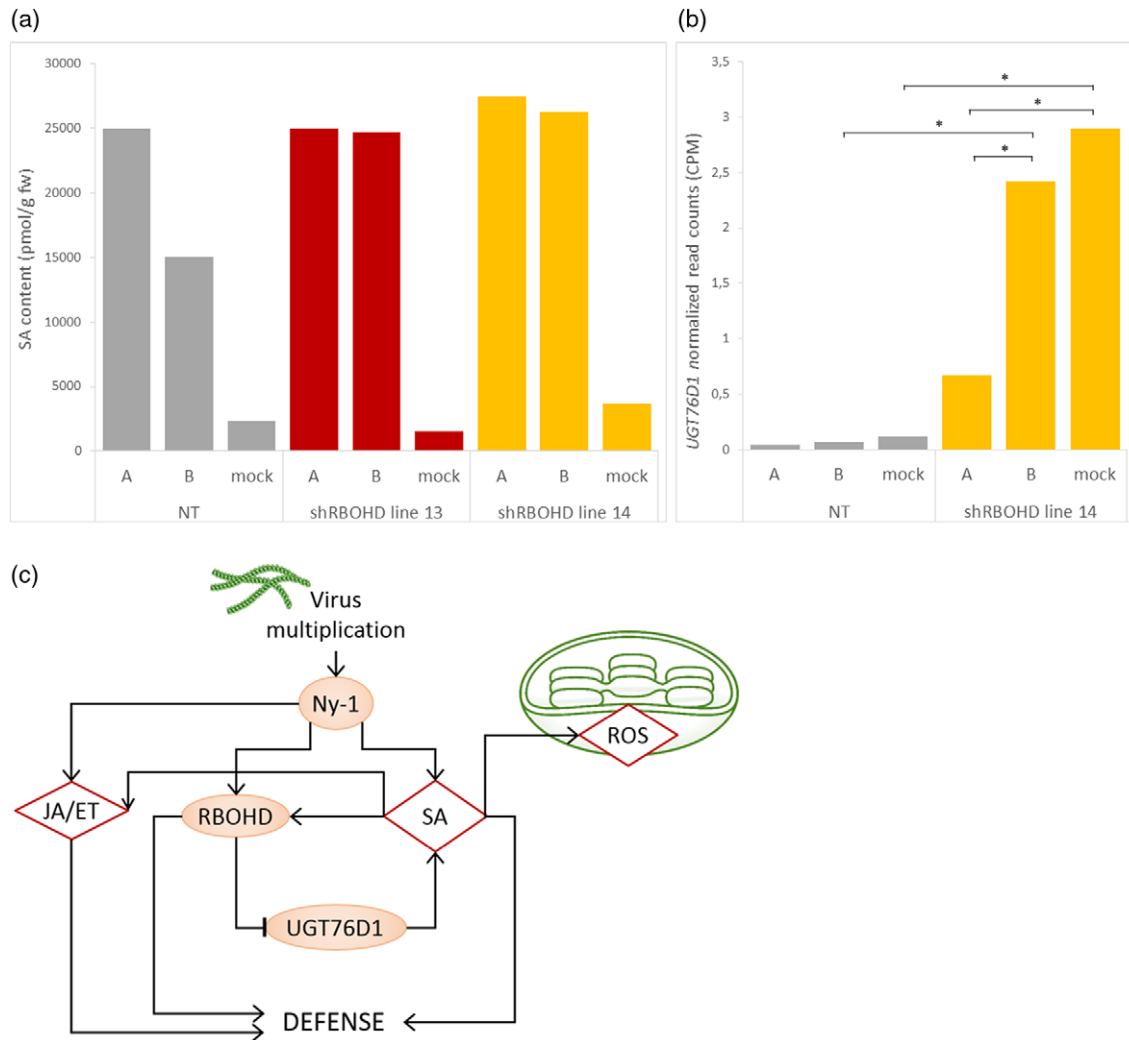


**Figure 7.** Functional *RBOHD* contributes to the spatial regulation of salicylic acid accumulation in potato resistance against potato virus Y. (a) Salicylic acid (SA) content was measured in the early stage of lesion development in non-transgenic (NT) and *RBOHD*-silenced (shRBOHD) plants within the lesion (section A) and in the tissue surrounding the lesion (section B) in comparison with mock-inoculated sections. Pools of 50–100 tissue sections from between six and eight plants were analyzed. Detailed data are shown in Data S5. (b) Expression of UDP-glucosyltransferase (*UGT76D1*) within the lesion (section A), its close surroundings (section B) and sections of mock-inoculated plants of NT and shRBOHD plants, as determined by RNA-seq analysis. The bar graph presents the average normalized read counts (CPM) of the *UGT76D1* gene across three biological replicates. Asterisks represent statistically significant differences among comparisons (false discovery rate-adjusted  $P < 0.05$ ). (c) SA synthesis and *RBOHD* are interconnected through a regulatory feedback loop. SA regulates *RBOHD* expression and, on the other hand, *RBOHD* is, through *UGT76D1*, involved in the spatial distribution of SA accumulation. SA regulates the chloroplastic production of reactive oxygen species. Signaling proteins are presented as orange ovals and metabolites as red diamonds. JA/ET, jasmonic acid/ethylene signaling; Ny-1, R protein; ROS, reactive oxygen species.

underlie the higher levels of SA detected in section B of transgenic lines (Figure 7b).

## DISCUSSION

The mechanism of the activation of R proteins and their interactions with effectors has been the subject of intensive research in recent years (Baggs *et al.*, 2017; Kourelis and Van Der Hoorn, 2018; Zhou and Zhang, 2020). To work towards sustainable resistance in the field, where the plant is also exposed to other environmental stressors, understanding the downstream processes leading

to pathogen arrest is of importance to balance the trade-offs between growth and immunity, however. To date, most of the studies of those processes have been performed in the model plant *Arabidopsis* (Piquerez *et al.*, 2014). Although some findings can be transferred to crop species using orthology (Lee *et al.*, 2015a; Ramšak *et al.*, 2018), this is not always the case, as in the recently reported redundancy of *PAD4* in Solanaceae, for example (Gantner *et al.*, 2019). Therefore, it is important to also perform the studies in crop plants, such as the potato.

	PROCESS	BIN	No. of genes	B vs. A		
				NT	shRboHD	NahG
Photosynthesis light reactions	photosystem II - LHClI	1.1.1.1	31	+		+
	photosystem II polypeptide units	1.1.1.2	107	+	+	+
	photosystem I polypeptide units	1.1.2.2	31		+	+
	NADH dehydrogenase	1.1.6	27	+	+	+
	cyclic electron flow-chlororespiration	1.1.40	41			+
Lipid and amino acid metabolism	lipid $\beta$ -oxidation - acyl-CoA reductase	11.9.4.13	27	-	-	
	histidine degradation	13.2.7	32		-	
Secondary metabolism	isoprenoids - mevalonate pathway	16.1.2	10			+
	flavonoids - chalcone synthase	16.8.2.1	13			+
PR proteins	PR-3, 4, 8, 11 (chitinases, chitin-binding proteins)	20.1.7.3	43		-	
Enzyme families	glutathione-S-transferases	26.9	43			-
	plastocyanin-like	26.19	48	-	-	-
	sulfotransferase	26.25	89			+
Transcription factors	basic helix-loop-helix family (BHLH)	27.3.6	29			+
	MYB-related transcription factor family	27.3.26	189		+	
Protein metabolism	ribosomal proteins	29.2.1.99.99	67	+	+	+
	receptor-like cytoplasmatic kinase VII	29.4.1.57	58		-	
	protein degradation	29.5	157		+	
	ubiquitination - proteasome	29.5.11.20	72			-
	serine protease	29.5.5	152			+
	protein assembly and cofactor ligation	29.8	74	+	+	+
Signalling	light signalling	30.11	156		+	+
	receptor kinases DUF26	30.2.17	93			-
Cell	vesicle transport	31.4	202		-	-
Transport	P- and V-type ATPases	34.1	45			-
	nucleotides	34.1	46			+
	peptides and oligopeptides	34.13	122		+	+

**Figure 8.** *RBOHD* contributes to the spatial regulation of processes in potato resistance signaling against viruses.

Differentially regulated processes between the lesion (section A) and the surrounding tissue (section B) of non-transgenic plants (NT), plants with perturbed SA accumulation (NahG) or plants with reduced *RBOHD* expression (shRBOHD). Only statistically significant (false discovery rate-corrected  $Q < 0.05$ ) enriched gene sets determined by gene set enrichment analysis (GSEA) in at least one comparison are presented. Process groups and individual processes together with MAPMAN bin names and the numbers of genes in the respective bin are shown. '+', induced processes; '-', repressed processes; blanks denote that a current process was not statistically significantly enriched.

Pathogen-infected leaf tissue comprises a heterogeneous mixture of host cells in different stages of defense response as a result of pathogen and defense signal movement from the primary infected cell (Maule *et al.*, 2002). Recently, spatially resolved transcriptome profiling in plant tissues has gained importance in unraveling complex regulatory networks (Giacomello *et al.*, 2017; Shulse *et al.*, 2019). The progressive and asynchronous effects of viral infection on host gene expression in relation to the spatial distribution of the virus have been investigated previously, but in compatible interactions (Aranda *et al.*, 1996; Escaler *et al.*, 2000; Maule *et al.*, 2002; Yang *et al.*, 2007). In resistance, however, the spatial distribution of a limited number of components has been studied only in model plants (Antoniw and White, 1986; Mur *et al.*, 1997; Betsuyaku *et al.*, 2018; Giolai *et al.*, 2019). Our approach to the analysis of small tissue sections presents a step forward in

studying the resistance response against the virus, and enabled the identification of a novel key player and the interconnectivity of components of immune signaling.

In the immune response, ROS are generated in two phases (Herrera-Vasquez *et al.*, 2015). The first, low-amplitude and transitory phase occurs within minutes of infection. The ROS generated at this stage are mostly apoplastic, tightly linked to the post-translational activation of plasma membrane RBOH NADPH oxidases (e.g. AtRBOHD and AtRBOHF) and cell wall peroxidases, and are attributed to PTI. (Torres, 2010; Shapiguzov *et al.*, 2012; Kadota *et al.*, 2019). The second, high-amplitude and sustained phase takes place a few hours after infection and depends on ROS generation in multiple compartments, including the apoplast, chloroplasts, mitochondria and peroxisomes. This second phase is linked to ETI and requires the transcriptional activation of *RBOH* genes (Shapiguzov

*et al.*, 2012). The role of RBOH proteins as the principal generator of ROS after pathogen attack was mostly studied in compatible interactions with bacterial and oomycete pathogens, using mutant and transgenic lines (Allan *et al.*, 2001; Torres *et al.*, 2002; Yoshioka *et al.*, 2003; Peer *et al.*, 2011), but also in symbiotic interaction with rhizobia (Yu *et al.*, 2018). Our spatiotemporal analysis of responses revealed that potato *RBOHD* (ortholog of *AtRBOHD*) is transcriptionally induced at the border region between virus-replicating and healthy cells around the cell death zone in the resistance response (Figure 4). Several studies have pointed to the essential role of ROS also in HR-conferred virus resistance (reviewed in Hernández *et al.*, 2016), including in one of the most studied viral pathosystems between *Nicotiana tabacum* (tobacco) and the tobacco mosaic virus (TMV) (Mur *et al.*, 1997; Liao *et al.*, 2015). Although the induction of *RBOHD* in the potato–PVY interaction has been shown previously (Otulak-Kozielec *et al.*, 2019), its role in the resistance response has not been studied functionally. We directly confirmed its essential role in potato resistance signaling, as *RBOHD*-silenced transgenic plants were not able to arrest the spread of the virus (Figure 6a,c). Besides the effect on cell-to-cell movement, both SA and *RBOHD* also have an effect on the efficiency of viral infection. The number of established foci of viral infection was the highest in NahG plants followed by *RBOHD*-silenced plants, whereas the lowest number of viral foci appeared in non-transgenic plants (Figure 6d). These results could imply a stronger impact of SA in immune signaling compared with *RBOHD*; however, one must note that NahG reduces the levels of SA to <10% of native values, whereas *RBOHD* is silenced to approximately 50% of its native transcriptional activity in our transgenic lines (Figure 6b).

Although the oxidative burst following pathogen recognition occurs in the apoplast, being generated mostly by RBOH proteins and cell wall peroxidases, pathogen-induced ROS can be also produced in other cellular compartments like mitochondria, chloroplasts and peroxisomes (reviewed in Sharma *et al.*, 2012; Mignolet-Spruyt *et al.*, 2016). Our comparative analysis of NT and NahG genotypes shows that the extensive production of ROS corresponds to the spread of the virus and/or PCD (Figure 5; Lukan *et al.*, 2018). The extensive ROS response in later stages of infection is most likely of non-apoplastic origin, as ROS production did not correspond to the expression of *RBOH* genes in NahG plants (Figures 5b and 6b). This is also supported by the expression pattern of ROS quenchers *CAT1* and *PRX28*, which are induced more distantly from the virus foci in NahG compared with NT plants (Figure 4). As SA was shown to be required for the generation of mitochondrial ROS during pathogen infection (Liao *et al.*, 2015), chloroplasts are its most probable source in our system. Transcriptional downregulation of photosynthesis genes leads to the generation of chloroplast ROS,

which were proposed as a signal orchestrating PCD (Zurbriggen *et al.*, 2010; Su *et al.*, 2018). In our pathosystem the transcriptional downregulation of photosynthesis genes was observed (Baebler *et al.*, 2014), and thus we can assume that, consequently, chloroplastic ROS are generated. Our results of H<sub>2</sub>O<sub>2</sub> staining (Figure 5a,b) are in agreement with the hypothesis that chloroplastic ROS stimulates localized cell death. Moreover, as the stained area was limited around the lesions in plants exhibiting resistance, but not in SA-depleted plants (Figure 5c), we suggest that SA regulates chloroplastic H<sub>2</sub>O<sub>2</sub> production.

The studies in Arabidopsis could not unambiguously determine the role of SA in the initiation of pathogen-induced PCD. In some pathosystems PCD can be regulated by SA, but not in all (Huysmans *et al.*, 2017; Radojičić *et al.*, 2018). Here, we determined that features of HR PCD are not dependent on SA in our studied pathosystem (Figures 3 and 6d). Moreover, this study provides the first detailed spatiotemporal ultrastructural analysis of HR PCD in potato following *Potyvirus* infection. We observed typical features of PCD and autophagy on the border of early and fully developed lesions (Figure 3). Similar features were previously observed in different pathosystems resulting either in susceptible or resistant plant–*Potyvirus* interaction (Hinrichs-Berger *et al.*, 1999; Otulak and Grazyna, 2012; Zielińska *et al.*, 2012; Choi *et al.*, 2016), supporting the hypothesis that the mechanisms of PCD are independent of the resistance mechanism (Künstler *et al.*, 2016). This is also in line with a recent study revealing that the activation of NLR proteins can directly lead to cell lysis through the insertion of resistosome into plasma membrane (Wang *et al.*, 2019).

Reactive oxygen species (ROS) were also proposed to be a central component of a self-amplifying loop that regulates the interaction balance between different phytohormones such as SA, JA and ET (reviewed in Torres, 2010). SA regulates RBOHD-dependent ROS production in Arabidopsis (reviewed in Liu and He, 2016). The same is true for our pathosystem, as the induction of *RBOHD* expression was significantly reduced after PVY inoculation in NahG plants (Figures 6b and S10b; Data S1). In Arabidopsis, *RBOHD* knockout mutant plants accumulated higher levels of SA following interaction with pathogens (Pogany *et al.*, 2009). On the other hand, Chaouch *et al.* (2012) did not detect any difference in SA accumulation in the *RBOHD* mutant compared with wild-type Arabidopsis (Chaouch *et al.*, 2012). We showed that in the potato–PVY interaction, SA biosynthesis is not controlled by RBOHD-generated ROS, as the concentration of SA in transgenic plants with silenced *RBOHD* did not differ significantly from SA concentration in NT plants at the site of viral foci. *RBOHD* is, however, involved in the spatial control of its accumulation (Figure 7a,c), confirming the existence of complex regulatory feedback loops. Indeed, UDP-glucosyltransferase (*UGT76D1*) was identified as a component of the feedback activation loop of SA

biosynthesis (Huang *et al.*, 2018) and our results show that it is spatially repressed by *RBOHD* signaling, explaining the regulation of SA accumulation (Figure 7b,c).

For efficient immunity the plant needs to block pathogen multiplication and spread, and at the same time limit the extent of damaged tissue and energy consumption. Thus the tight spatial regulation of these processes is of utmost importance. It has been long assumed that positive regulators act at the HR site and negative regulators act in the surrounding areas, but the molecular evidence for this premise is mostly lacking through a lack of functional zonation studies (Huysmans *et al.*, 2017). We show here that *RBOHD* and SA regulate the immune response in a spatio-diverse manner, leading to the fine-tuning of both spatial and temporal responses.

## EXPERIMENTAL PROCEDURES

### Plant material

Potato (*Solanum tuberosum* L.) plants cv. Rywal and NahG-Rywal (Baebler *et al.*, 2014) and derived transgenic lines (see below) were grown and inoculated with PVY<sup>NTN</sup> (isolate NIB-NTN, AJ585342), PVY<sup>N-Wilga</sup> (PVYN-Wi; EF558545) or PVY<sup>N605</sup>, tagged with green fluorescent protein (PVY<sup>N</sup>-GFP) (Jakab *et al.*, 1997; Dietrich and Maiss, 2003; Rupar *et al.*, 2015) or mock inoculated, as described by Baebler *et al.* (2009).

### qPCR gene expression analysis in tissue sections

For gene expression analyses lesions at two different stages were sampled (see Figure 1a). For each lesion, four tissue sections were sampled (Figure 1a). Tissue sections were stored in 100  $\mu$ l of RNA-later RNA Stabilization Solution (ThermoFisher Scientific, <https://www.thermofisher.com>). Altogether, five independent experiments were performed, each comprising of approximately 20 plants per experimental group. For each experimental group, between five and 10 lesions from different plants were sampled (Table S2).

Standard gene expression analysis procedures were optimized for the analysis of small leaf sections. Fixed tissue sections were homogenized using Tissue Lyser (Qiagen, <https://www.qiagen.com>), followed by RNA isolation using the RNeasy Plant Micro Kit (Qiagen), DNase treatment, quality control and reverse transcription.

The expression of 23 genes involved in different steps of immune signaling (Figure 1c) was analyzed and normalized to the expression of two validated reference genes, *COX* and *18S*, as described previously (Petek *et al.*, 2014; for primer and probe information and full experimental details, see Table S3), to eliminate technical variability, including the effect of different quantities of RNA in tissue sections. The standard curve method was used for relative gene expression quantification using QUANTGENIUS (<http://quantgenius.nib.si>; Baebler *et al.*, 2017).

### Statistical modeling of tissue section qPCR gene expression data

Prior to a statistical analysis of the gene expression dataset for tissue sections, data from lesions without viral amplification detected in section A (i.e. necrosis cause by mechanical inoculation) were filtered out. Relative gene expression values were next standardized

to the 97th quantile of the maximum value across all samples (for inoculated and mock samples in both studied genotypes). The multiple linear regression method, as implemented in the R package STATS (R Core Team, 2020), was used to fit a quadratic polynomial model, with genotype and position (tissue section) or measured distance from position A (initial viral foci tissue surrounding) included as factors. An analysis of variance (ANOVA) was additionally used to analyze the effects of position and genotype on gene expression. For each gene analyzed, spatial expression profiles were determined and plotted with 95% confidence intervals. For data for the early visible lesions, calculations were performed for both perpendicular directions and their average, respectively. Expression changes between genotypes at different times post-inoculation were further visualized using coefficient plots, with linear coefficients plotted on the x-axis and quadratic coefficients plotted on the y-axis. The significance of comparisons between the levels of the factors was obtained through the contrast method as implemented in the R package LIMMA.

### Gene expression in whole leaves

For the gene expression analysis in whole leaves of different genotypes, including newly constructed transgenic lines (see the experimental set-ups below), whole leaves were sampled. RNA was isolated and reverse transcription and qPCR was performed as described previously (Baebler *et al.*, 2014), with normalization to COX only. Where applicable, a Student's *t*-test (in EXCEL) was used to compare treatments.

### RNA-seq analysis in tissue sections

For RNA-seq, early visible lesions were sampled from PVY<sup>N-Wilga</sup>-inoculated leaves of cv. Rywal, NahG-Rywal and shRBOHD (line 14) plants. Thirty tissue sections of the lesion (A) and its immediate surroundings (B; Figure 1a) were collected and pooled separately (pool A and pool B). Sections of mock-inoculated plants were prepared as described above and pooled (with approximately 300 sections per pool). The pools were stored and homogenized as described above. RNA extraction and library preparation are described in Method S1. RNA-seq was performed on the HiSeq platform (Illumina, <https://www.illumina.com>) using 150-bp paired-end reads at Novogene (<https://en.novogene.com>) or LC Sciences (<https://www.lcsciences.com>). Quality control was performed in CLC GENOMICS WORKBENCH 12.0 (Qiagen). The merging of overlapping pairs, the mapping of reads to the potato genome (Petek *et al.*, 2020) and read counting were performed in both CLC GENOMICS and STAR. Differential expression analysis was performed in R (R Core Team, 2020; version 3.2.2), using the R package LIMMA (Ritchie *et al.*, 2015), trimmed mean of M values (TMM) normalization and voom function. Adjusted *P* values below 0.05 were considered statistically significant. For full experimental details, see Method S1. Raw and normalized RNA-seq data were deposited to the Gene Expression Omnibus (GEO, accession number GSE142002, <https://www.ncbi.nlm.nih.gov/geo/query/acc.cgi?acc=GSE142002>).

Gene set enrichment analysis (GSEA; Subramanian *et al.*, 2005) was performed to search for groups of genes involved in the same processes that were significantly (false discovery rate-corrected  $Q < 0.05$ ) altered by virus inoculation, using MapMan ontology as the source of the gene sets (obtained from GoMapMan database; Ramšak *et al.*, 2014).

### Construction of short hairpin RNA transgenics

Primers were designed based on a consensus sequence obtained by sequence alignment of sequences of *RBOHD* genes

(Sotub06g025550 and Sotub06g025580) (Figure S14). cDNA obtained from cv. Rywal was used as a template for the amplification of the 436-bp-long fragment of the *RBOHD* gene. The product was cloned into the pENTR D-TOPO plasmid and sequenced. The fragment was further transferred to pH7GWIWG2, sequenced and electroporated into *Agrobacterium tumefaciens* LBA4404 that was used for the transformation of cv. Rywal plantlets (for full experimental details, see the legend to Figure S14). Silencing efficacy was analyzed in one leaf per transgenic line by qPCR using shRBOHD primers (Table S3) as a target, as described above.

### Phenotypization

Lesions that developed on virus-inoculated leaves of cv. Rywal, NahG-Rywal and two short hairpin transgenic lines with silenced RBOHD (lines 13 and 14) inoculated with PVY<sup>N</sup>-GFP or mock inoculated were counted from 3 to 14 dpi (for the numbers of plants tested for each experiment, see Data S4). The number of lesions was calculated per cm<sup>2</sup> of leaf area. For the same plants, the times of lesion appearance on non-inoculated leaves was also recorded.

Viral quantity was analyzed in the same genotypes as above at 6 dpi in the inoculated leaves and at 24 and 39 dpi in non-inoculated leaves (using between one and three leaves from up to five plants). Sample preparation and qPCR analysis were performed as described above using PVY as a target gene. The experiment was repeated three times.

The lesion diameter was measured in the images of individual leaves of cv. Rywal and NahG-Rywal, inoculated with PVY<sup>N-Wilga</sup> or PVY<sup>NTN</sup>, in PHOTOSHOP CS3 (Adobe, <https://www.adobe.com>) and standardized to leaf diameter. The experiment was repeated twice.

### H<sub>2</sub>O<sub>2</sub> staining

Leaves (three leaves from three plants per genotype/treatment) of Rywal and NahG-Rywal plants, inoculated with PVY<sup>NTN</sup> or mock inoculated, were sampled 3–8 days after inoculation and stained with 3,3'-diaminobenzidine (DAB) staining solution (for full experimental details, see Method S2). Diameters of lesions and DAB staining areas were measured on spatially calibrated images in FIJI (Schindelin *et al.*, 2012). The difference in the diameter of lesion and the DAB area was measured for each individual lesion. Data were analyzed in R 3.5.0 (R Core Team, 2020), and statistical significance was tested with ANOVA and Tukey's *post-hoc* test ( $P = 0.05$ ).

### Transmission electron microscopy

Ultrastructural changes following PVY<sup>NTN</sup> and PVY<sup>N-Wilga</sup> inoculation of the cells in and around the early visible and fully developed lesions were observed in Rywal and NahG-Rywal using transmission electron microscopy (TEM; Philips CM 100). A tissue section including a lesion and surrounding cells was cut from inoculated leaves and prepared as described in Method S3. To estimate the lesion size in each genotype, cross-sections of the leaves were analyzed by TEM. The average lesion size was determined by counting the number of dead cells in the diameter of approximately 15 lesions for each genotype.

### Hormonal measurements

Both SA and JA contents were determined in non-transgenic cv. Rywal and two short hairpin transgenic lines with silenced *RBOHD* (lines 13 and 14) at 4 dpi after PVY<sup>N-Wilga</sup> or mock inoculation. Between 60 and 130 sections containing initial virus foci (section A) and surrounding tissue (section B) were

sampled from the third inoculated leaf from between six and eight plants for each genotype. Hormones were isolated and measured by gas chromatography coupled with mass spectrometry (GC-MS) as described by Križnik *et al.* (2017).

### DATA AVAILABILITY

Raw and normalized RNA-seq data were deposited in GEO (accession number GSE142002, <https://www.ncbi.nlm.nih.gov/geo/query/acc.cgi?acc=GSE142002>). All other relevant data can be found within the article and its supporting material.

### ACKNOWLEDGEMENTS

The authors thank Dr John Carr for a critical review of the manuscript and Maja Gnezda, Neža Turnšek and Lidija Matičič for technical assistance.

### AUTHOR CONTRIBUTIONS

ŠB, MPN, KG, TL AND JH designed the research. ŠB, MPN, KG, TL, MTŽ, AK, KS, BD, AC, SP, KM and MK performed the research. TL, ŠB, AK, MTŽ, AB, MZ, KG, MK and SP analyzed the data. TL, ŠB, AK, MZ, KG, MK, MPN, MTŽ, BD, AC and JH contributed to the writing or revision of the article.

### CONFLICT OF INTEREST

The authors declare that they have no conflicts of interest.

### SUPPORTING INFORMATION

Additional Supporting Information may be found in the online version of this article.

**Figure S1.** Lesions appear systemically if Ny-gene-conferred resistance is perturbed in SA signaling.

**Figure S2.** Lesion diameter is twofold larger in NahG compared with NT plants following inoculation with PVY.

**Figure S3.** Transcriptional response of selected immune signaling-related genes and relative viral RNA abundance are similar after inoculation with different viral strains.

**Figure S4.** Spatiotemporal gene expression of immune signaling genes.

**Figure S5.** 3D representation of spatial gene expression response to PVY inoculation at the time of fully developed lesions.

**Figure S6.** 3D representation of spatial gene expression response to PVY inoculation at the time of early visible lesions.

**Figure S7.** 3D animated spatial gene expression of immune signaling genes around early visible lesions.

**Figure S8.** 9-LOX and 13-LOX branches of the oxylipin pathway respond differentially in potato resistance against PVY.

**Figure S9.** Programmed cell death in the center of a fully developed lesion after PVY infection.

**Figure S10.** The virus is present in symptomatic non-inoculated leaves of plants of RBOHD-silenced transgenic lines.

**Figure S11.** Performance of *RBOHD*-silenced plant inoculated leaves after PVY inoculation?

**Figure S12.** Spatial transcriptional response is similar in shRBOHD and NahG genotypes.

**Figure S13.** Spatial expression of UDP-glucosyltransferase (*UGT76D1*) in different genotypes.

**Figure S14.** Construction of short hairpin RNA transgenics.

**Table S1.** Gene expression changes of selected genes in whole-leaf homogenates at different time points after inoculation with PVY.

**Table S2.** Independent experiments performed for targeted spatiotemporal gene expression analyses.

**Table S3.** Selected genes and corresponding primers and probe sequences for expression analyses with quantitative PCR.

**Methods S1.** RNA-seq analysis.

**Methods S2.** H<sub>2</sub>O<sub>2</sub> staining and imaging.

**Methods S3.** Transmission electron microscopy.

**Data S1.** Standardized qPCR gene expression data.

**Data S2.** Results of statistical modeling of tissue section gene expression data.

**Data S3.** Individual lesion sizes.

**Data S4.** Number of lesions on inoculated leaves of different potato genotypes following PVY inoculation.

**Data S5.** Hormonal contents in tissue sections of different potato genotypes.

**Data S6.** Results of spatial RNA-seq analysis of Rywal, NahG and shRBOHD genotypes following PVY<sup>N-Wilga</sup> inoculation.

## OPEN RESEARCH BADGES



This article has earned an Open Data badge for making publicly available the digitally-shareable data necessary to reproduce the reported results. The data is available at <https://www.ncbi.nlm.nih.gov/geo/query/acc.cgi?acc=GSE142002>.

## REFERENCES

- Allan, A.C., Lapidot, M., Culver, J.N. and Fluhr, R. (2001) An early tobacco mosaic virus-induced oxidative burst in tobacco indicates extracellular perception of the virus coat protein. *Plant Physiol.* **126**, 97–108. <https://doi.org/10.1104/pp.126.1.97>.
- Antoniw, J.F. and White, R.F. (1986) Changes with time in the distribution of virus and PR protein around single local lesions of TMV infected tobacco. *Plant Mol. Biol.* **6**(3), 145–149. <https://doi.org/10.1007/bf00021483>.
- Aranda, M.A., Escaler, M., Wang, D. and Maule, A.J. (1996) Induction of HSP70 and polyubiquitin expression associated with plant virus replication. *Proc. Natl Acad. Sci. USA*, **93**, 15289–15293.
- Baebler, S., Krečić-Stres, H., Rotter, A. et al. (2009) PVY(NTN) elicits a diverse gene expression response in different potato genotypes in the first 12 h after inoculation. *Mol. Plant Pathol.* **10**, 263–275. <https://doi.org/10.1111/j.1364-3703.2008.00530.x>.
- Baebler, S., Svalina, M., Petek, M., Stare, K., Rotter, A., Pompe-Novak, M. and Gruden, K. (2017) QuantGenius: implementation of a decision support system for qPCR-based gene quantification. *BMC Bioinformatics*, **18**, 276. <https://doi.org/10.1186/s12859-017-1688-7>.
- Baebler, S., Witek, K., Petek, M. et al. (2014) Salicylic acid is an indispensable component of the Ny-1 resistance-gene-mediated response against Potato virus Y infection in potato. *J. Exp. Bot.* **65**, 1095–1109. <https://doi.org/10.1093/jxb/ert447>.
- Baggs, E., Dagdas, G. and Krasileva, K.V. (2017) ScienceDirect NLR diversity, helpers and integrated domains: making sense of the NLR IDentity. *Curr. Opin. Plant Biol.* **38**, 59–67.
- Balint-Kurti, P. (2019) The plant hypersensitive response: concepts, control and consequences. *Mol. Plant Pathol.* **20**, 1163–1178. <https://doi.org/10.1111/mpp.12821>.
- Betsuyaku, S., Katou, S., Takebayashi, Y., Sakakibara, H., Nomura, N. and Fukuda, H. (2018) Salicylic acid and jasmonic acid pathways are activated in spatially different domains around the infection site during effector-triggered immunity in *Arabidopsis thaliana*. *Plant and Cell Physiol.* **59**, 8–16. <https://doi.org/10.1093/pcp/pcx181>.
- Breen, S., Williams, S.J., Outram, M., Kobe, B. and Solomon, P.S. (2017) Emerging Insights into the functions of pathogenesis-related protein 1. *Trends Plant Sci.* **22**, 871–879. <https://doi.org/10.1016/j.tplants.2017.06.013>.
- Calil, I.P. and Fontes, E.P.B. (2017) Plant immunity against viruses: antiviral immune receptors in focus. *Ann. Bot.* **119**, 711–723. <https://doi.org/10.1093/aob/mcw200>.
- Chaouch, S., Queval, G. and Noctor, G. (2012) AtRbohF is a crucial modulator of defence-associated metabolism and a key actor in the interplay between intra-cellular oxidative stress and pathogenesis responses in *Arabidopsis*. *Plant J.* **69**, 613–627. <https://doi.org/10.1111/j.1365-313X.2011.04816.x>.
- Chivasa, S. and Carr, J.P. (1998) Cyanide restores N gene-mediated resistance to tobacco mosaic virus in transgenic tobacco expressing salicylic acid hydroxylase. *Plant Cell*, **10**, 1489–1498. <https://doi.org/10.1105/tpc.10.9.1489>.
- Chivasa, S., Murphy, A.M., Naylor, M. and Carr, J.P. (1997) Salicylic acid interferes with tobacco mosaic virus replication via a novel salicylhydroxamic acid-sensitive mechanism. *Plant Cell*, **9**, 547–557. <https://doi.org/10.1105/tpc.9.4.547>.
- Choi, D., Park, J., Oh, S. and Cheong, H. (2016) Autophagy induction in tobacco leaves infected by potato virus YO and its putative roles. *Biochem. Biophys. Res. Commun.* **474**, 606–611. <https://doi.org/10.1016/j.bbrc.2016.03.104>.
- Dickman, M.B. and de Figueiredo, P. (2013) Death be not proud — cell death control in plant fungal interactions. *PLoS Pathog.* **9**, e1003542. <https://doi.org/10.1371/journal.ppat.1003542>.
- Dietrich, C. and Maiss, E. (2003) Fluorescent labelling reveals spatial separation of potyvirus populations in mixed infected *Nicotiana benthamiana* plants. *J. Gen. Virol.* **84**, 2871–2876. <https://doi.org/10.1099/vir.0.19245-0>.
- Dorey, S., Baillieux, F., Pierrel, M., Saindrenan, P., Fritig, B., De, B.I. and Pasteur, U.L. (1997) Spatial and temporal induction of cell death, defense genes, and accumulation of salicylic acid in tobacco leaves reacting hypersensitively to a fungal glycoprotein elicitor. *MPMI*, **10**, 646–655.
- Escaler, M., Aranda, M.A., Thomas, C.L. and Maule, A.J. (2000) Pea embryonic tissues show common responses to the replication of a wide range of viruses. *Virology*, **267**, 318–325. <https://doi.org/10.1006/viro.1999.0119>.
- Gantner, J., Ordon, J., Kretschmer, C., Guerois, R. and Stuttmann, J. (2019) An EDS1-SAG101 complex is essential for TNL-mediated immunity in *Nicotiana benthamiana*. *Plant Cell*, **31**, 2456–2474. <https://doi.org/10.1105/tpc.19.00099>.
- Giacomello, S., Salmén, F., Terebieniec, B.K. et al. (2017) Spatially resolved transcriptome profiling in model plant species. *Nat. Plants*, **3**, 17061. <https://doi.org/10.1038/nplants.2017.61>.
- Giolai, M., Verweij, W., Lister, A., Heavens, D., MacAulay, I. and Clark, M.D. (2019) Spatially resolved transcriptomics reveals plant host responses to pathogens. *Plant Methods*, **15**, 114. <https://doi.org/10.1186/s13007-019-0498-5>.
- Havelda, Z. and Maule, A.J. (2000) Complex spatial responses to cucumber mosaic virus infection in susceptible cucurbita pepo cotyledons. *Plant Cell*, **12**, 1975–1985.
- Hernández, J.A., Gullner, G., Clemente-Moreno, M.J., Künstler, A., Juhász, C., Diaz-Vivancos, P., Király, L. (2016) Oxidative stress and antioxidative responses in plant-virus interactions. *Physiol. Mol. Plant Pathol.* **94**, 134–148. <https://doi.org/10.1016/j.pmp.2015.09.001>.
- Herrera-Vasquez, A., Salinas, P. and Holuigue, L. (2015) Salicylic acid and reactive oxygen species interplay in the transcriptional control of defense genes expression. *Front. Plant Sci.* **6**, 1–9. <https://doi.org/10.3389/fpls.2015.00171>.
- Hinrichs-Berger, J., Harfold, M., Berger, S. and Buchenauer, H. (1999) Cytological responses of susceptible and extremely resistant potato plants to inoculation with potato virus Y. *Physiol. Mol. Plant Pathol.* **55**, 143–150. <https://doi.org/10.1006/pmp.1999.0216>.
- Huang, X.X., Zhu, G.Q., Liu, Q., Chen, L., Li, Y.J. and Hou, B.K. (2018) Modulation of plant salicylic acid-associated immune responses via glycosylation of dihydroxybenzoic acids. *Plant Physiol.* **176**, 3103–3119. <https://doi.org/10.1104/pp.17.01530>.
- Huysmans, M., Lema, A. S., Coll, N.S. and Nowack, M.K. (2017) Dying two deaths — programmed cell death regulation in development and disease. *Curr. Opin. Plant Biol.* **35**, 37–44. <https://doi.org/10.1016/j.pbi.2016.11.005>.
- Jakab, G., Droz, E., Brigneti, G., Baulcombe, D. and Malnoe, P. (1997) Infectious in vivo and in vitro transcripts from a full-length cDNA clone of

- PVY-N605, a Swiss necrotic isolate of potato virus Y. *J. Gen. Virol.* **78**, 3141–3145.
- Jones, J.D.G. and Dangl, J.L. (2006) The plant immune system. *Nature*, **444**, 323–329. <https://doi.org/10.1038/nature05286>.
- Kadota, Y., Liebrand, T.W.H., Goto, Y. et al. (2019) Quantitative phosphoproteomic analysis reveals common regulatory mechanisms between effector- and PAMP-triggered immunity in plants. *New Phytol.* **221**, 2160–2175. <https://doi.org/10.1111/nph.15523>.
- Kadota, Y. and Shirasu, K. (2012) The HSP90 complex of plants. *Biochim. Biophys. Acta*, **1823**, 689–697. <https://doi.org/10.1016/j.bbamcr.2011.09.016>.
- Karasev, A.V. and Gray, S.M. (2013) Continuous and emerging challenges of Potato virus Y in potato. *Annu. Rev. Phytopathol.* **51**, 571–586. <https://doi.org/10.1146/annurev-phyto-082712-102332>.
- Kourelis, J. and Van Der Hoorn, R.A.L. (2018) Defended to the nines: 25 years of resistance gene cloning identifies nine mechanisms for R protein function. *Plant Cell*, **30**, 285–299. <https://doi.org/10.1105/tpc.17.00579>.
- Kriznik, M., Petek, M., Dobnik, D., Ramsak, Z. and Baebler, S. (2017) Salicylic acid perturbs sRNA-gibberellin regulatory network in immune response of potato to potato virus Y infection. *Front. Plant Sci.* **8**, 2192. <https://doi.org/10.3389/fpls.2017.02192>.
- Künstler, A., Bacsó, R., Gullner, G., Hafez, Y.M. and Király, L. (2016) Staying alive - is cell death dispensable for plant disease resistance during the hypersensitive response? *Physiol. Mol. Plant Pathol.* **93**, 75–84. <https://doi.org/10.1016/j.pmp.2016.01.003>.
- Lacomme, C., Glais, L., Bellstedt, D., Dupuis, B., Karasev, A., Jacquot, E. (eds) (2017) *Bergey's Manual of Systematic Bacteriology*. New York: Springer-Verlag. <https://www.springer.com/gp/book/9783319588582> doi: 10.1007/978-3-319-58860-5.
- Lee, T., Kim, H. and Lee, I. (2015a) Network-assisted crop systems genetics: network inference and integrative analysis. *Curr. Opin. Plant Biol.* **24**, 61–70. <https://doi.org/10.1016/j.cpb.2015.02.001>.
- Lee, W.S., Devonshire, B.J., Hammond-Kosack, K.E., Rudd, J.J. and Kanyuka, K. (2015b) Deregulation of plant cell death through disruption of chloroplast functionality affects asexual sporulation of *Zymoseptoria tritici* on wheat. *Mol. Plant-Microbe Interact.* **28**, 590–604. <https://doi.org/10.1094/MPMI-10-14-0346-R>.
- Li, N., Han, X., Feng, D., Yuan, D. and Huang, L.J. (2019) Signaling crosstalk between salicylic acid and ethylene/Jasmonate in plant defense: Do we understand what they are whispering? *Int. J. Mol. Sci.* **20**, 671. <https://doi.org/10.3390/ijms20030671>.
- Liao, Y., Tian, M., Zhang, H. et al. (2015) Salicylic acid binding of mitochondrial alpha-ketoglutarate dehydrogenase E2 affects mitochondrial oxidative phosphorylation and electron transport chain components and plays a role in basal defense against tobacco mosaic virus in tomato. *New Phytol.* **205**, 1296–1307.
- Liu, Y. and He, C. (2016) Regulation of plant reactive oxygen species (ROS) in stress responses: learning from ATRBOHD. *Plant Cell Rep.* **35**, 995–1007. <https://doi.org/10.1007/s00299-016-1950-x>.
- Lukan, T., Baebler, S., Marusa, P.-N., Guček, K., Zagorščak, M., Coll, A. and Gruden, K. (2018) Cell death is not sufficient for the restriction of potato virus Y spread in hypersensitive response-conferred resistance in potato. *Front. Plant Sci.* **9**, 168. <https://doi.org/10.3389/fpls.2018.00168>.
- Maule, A., Leh, V. and Lederer, C. (2002) The dialogue between viruses and hosts in compatible interactions. *Curr. Opin. Plant Biol.* **5**, 279–284. [https://doi.org/10.1016/S1369-5266\(02\)00272-8](https://doi.org/10.1016/S1369-5266(02)00272-8).
- Mignolet-Spruyt, L., Xu, E., Idänheimo, N., Hoeberichts, F.A., Mühlenbock, P., Brosché, M., Van Breusegem, F. and Kangasjärvi, J. (2016) Spreading the news: subcellular and organellar reactive oxygen species production and signalling. *J. Exp. Bot.* **67**, 3831–3844. <https://doi.org/10.1093/jxb/erw080>.
- Morant, A.V., Jørgensen, K., Jørgensen, C., Paquette, S.M., Sánchez-Pérez, R., Möller, B.L. and Bak, S. (2008)  $\beta$ -Glucosidases as detonators of plant chemical defense. *Phytochemistry*, **69**, 1795–1813. <https://doi.org/10.1016/j.phytochem.2008.03.006>.
- Mur, L.A.J., Bi, Y.-M., Darby, R.M., Firek, S. and Draper, J. (1997) Compromising early salicylic acid accumulation delays the hypersensitive response and increases viral dispersal during lesion establishment in TMV-infected tobacco. *Plant J.* **12**, 1113–1126. <https://doi.org/10.1046/j.1365-3113.1997.12051113.x>.
- Mur, L.A.J., Kenton, P., Lloyd, A.J., Ougham, H. and Prats, E. (2008) The hypersensitive response; the centenary is upon us but how much do we know? *J. Exp. Bot.* **59**, 501–520. <https://doi.org/10.1093/jxb/ern239>.
- Niehl, A., Wyrsh, I., Boller, T. and Heinlein, M. (2016) Double-stranded RNAs induce a pattern-triggered immune signaling pathway in plants. *New Phytol.* **211**, 1008–1019. <https://doi.org/10.1111/nph.13944>.
- Otulak-Kozielec, K., Kozielec, E. and Valverde, R.A. (2019) The respiratory burst oxidase homolog D (RbohD) cell and tissue distribution in potato-potato virus Y (PVYNTN) hypersensitive and susceptible reactions. *Int. J. Mol. Sci.* **20**, 2741. <https://doi.org/10.3390/ijms2012741>.
- Otulak, K. and Grazyna, G. (2012) Cytopathological potato virus Y structures during solanaceous plants infection. *Micron*, **43**, 839–850. <https://doi.org/10.1016/j.micron.2012.02.015>.
- Peer, M., Bach, M., Mueller, M.J. and Waller, F. (2011) Free sphingobases induce RBOHD-dependent reactive oxygen species production in Arabidopsis leaves. *FEBS Lett.* **585**, 3006–3010. <https://doi.org/10.1016/j.febslet.2011.08.016>.
- Petek, M., Rotter, A., Kogovšek, P., Baebler, S., Mithöfer, A. and Gruden, K. (2014) Potato virus Y infection hinders potato defence response and renders plants more vulnerable to Colorado potato beetle attack. *Mol. Ecol.* **23**, 5378–5391. <https://doi.org/10.1111/mec.12932>.
- Petek, M., Zagorščak, M., Ramsak, Z., Sanders, S., Tomaž, S., Tseng, E., Zouine, M., Coll, A. and Gruden, K. (2020) Cultivar-specific transcriptome and pan-transcriptome reconstruction of tetraploid potato. *Sci. Data*, **7**, 1–15. <https://doi.org/10.1038/s41597-020-00581-4>.
- Pieterse, C.M.J., Van der Does, D., Zamioudis, C., Leon-Reyes, A. and Van Wees, S.C.M. (2012) Hormonal modulation of plant immunity. *Annu. Rev. Cell Dev. Biol.* **28**, 489–521. <https://doi.org/10.1146/annurev-cellbio-092910-154055>.
- Piquerez, S.J.M., Harvey, S.E., Beynon, J.L. and Ntoukakis, V. (2014) Improving crop disease resistance: lessons from research on Arabidopsis and tomato. *Front. Plant Sci.* **5**, 1–13. <https://doi.org/10.3389/fpls.2014.00671>.
- Pogany, M., von Rad, U., Grun, S., Dongo, A., Pintye, A., Simoneau, P., Bahneweg, G., Kiss, L., Barna, B. and Durner, J. (2009) Dual roles of reactive oxygen species and NADPH oxidase RBOHD in an Arabidopsis-Alternaria pathosystem. *Plant Physiol.* **151**, 1459–1475. <https://doi.org/10.1104/pp.109.141994>.
- Quenouille, J., Vassilakos, N. and Moury, B. (2013) Potato virus Y: a major crop pathogen that has provided major insights into the evolution of viral pathogenicity. *Mol. Plant Pathol.* **14**(5), 439–452. <https://doi.org/10.1111/mpp.12024>.
- R Core Team (2020). *R: A Language and Environment for Statistical Computing*. Vienna: R Foundation for Statistical Computing. Available at: <http://www.R-project.org/>.
- Radojčić, A., Li, X. and Zhang, Y. (2018) Salicylic acid: a double-edged sword for programmed cell death in plants. *Front. Microbiol.* **9**, 1133. <https://doi.org/10.3389/fpls.2018.01133>.
- Ramsak, Z., Baebler, S., Rotter, A., Korbar, M., Mozetič, I., Usadel, B. and Gruden, K. (2014) GoMapMan: integration, consolidation and visualization of plant gene annotations within the MapMan ontology. *Nucleic Acids Res.* **42**, D1167–D1175. <https://doi.org/10.1093/nar/gkt1056>.
- Ramsak, Z., Coll, A., Stare, T., Tzfadia, O., Baebler, S., Van De, P.Y. and Gruden, K. (2018) Network modeling unravels mechanisms of crosstalk between ethylene and salicylate signaling in potato. *Plant Physiol.* **178**, 488–499. <https://doi.org/10.1104/pp.18.00450>.
- Ritchie, M.E., Phipson, B., Wu, D., Hu, Y., Law, C.W., Shi, W. and Smyth, G.K. (2015) Limma powers differential expression analyses for RNA-sequencing and microarray studies. *Nucleic Acids Res.* **43**, e47. <https://doi.org/10.1093/nar/gkv007>.
- Rupar, M., Faurez, F., Tribodet, M. et al. (2015) Fluorescently tagged Potato virus Y: a versatile tool for functional analysis of plant-virus interactions. *Mol. Plant-Microbe Interact.* **28**, 739–750. <https://doi.org/10.1094/MPMI-07-14-0218-TA>.
- Schindelin, J., Arganda-carreras, I., Frise, E. et al. (2012) Fiji - an open source platform for biological image analysis. *Nat. Methods*, **9**, 1–15. <https://doi.org/10.1038/nmeth.2019.fiji>.
- Shapiguzov, A., Julia, P., Wrzaczek, M. and Kangasjärvi, J. (2012) ROS-talk - how the apoplast, the chloroplast, and the nucleus get the message through. *Front. Plant Sci.* **3**, 292. <https://doi.org/10.3389/fpls.2012.00292>.



- Sharma, P., Jha, A.B., Dubey, R.S. and Pessaraki, M. (2012) Reactive oxygen species, oxidative damage, and antioxidative defense mechanism in plants under stressful conditions. *J. Bot.* **2012**, 1–26. <https://doi.org/10.1155/2012/217037>.
- Shulse, C.N., Cole, B.J., Ciobanu, D. *et al.* (2019) High-throughput single-cell transcriptome profiling of plant cell types. *Cell Rep.* **27**, 2241–2247. <https://doi.org/10.1016/j.celrep.2019.04.054>.
- Su, J., Yang, L., Zhu, Q., Wu, H., He, Y., Liu, Y., Xu, J., Jiang, D. and Zhang, S. (2018) Active photosynthetic inhibition mediated by MPK3/MPK6 is critical to effector-triggered immunity. *PLoS Biol.* **16**, e2004122.
- Subramanian, A., Tamayo, P., Mootha, V.K. *et al.* (2005) Gene set enrichment analysis: a knowledge-based approach for interpreting genome-wide expression profiles. *Proc. Natl Acad. Sci. USA*, **102**, 15545–15550. <https://doi.org/10.1073/pnas.0506580102>.
- Szajko, K., Chrzanowska, M., Witek, K., Strzelczyk-Zyta, D., Zagórska, H., Gebhardt, C., Hennig, J. and Marczewski, W. (2008) The novel gene Ny-1 on potato chromosome IX confers hypersensitive resistance to Potato virus Y and is an alternative to Ry genes in potato breeding for PVY resistance. *Theor. Appl. Genet.* **116**, 297–303. <https://doi.org/10.1007/s00122-007-0667-1>.
- Torres, M.A. (2010) ROS in biotic interactions. *Physiol. Plant*, **138**, 414–429. <https://doi.org/10.1111/j.1399-3054.2009.01326.x>.
- Torres, M.A., Dangl, J.L. and Jones, J.D.G. (2002) Arabidopsis gp91phox homologues AtrbohD and AtrbohF are required for accumulation of reactive oxygen intermediates in the plant defense response. *Proc. Natl Acad. Sci.* **99**, 517–522. <https://doi.org/10.1073/pnas.012452499>.
- Wang, J., Hu, M., Wang, J., Qi, J., Han, Z., Wang, G., Qi, Y., Wang, H.W., Zhou, J.M. and Chai, J. (2019) Reconstitution and structure of a plant NLR resistosome conferring immunity. *Science*, **364**(6435), <https://doi.org/10.1126/science.aav5870>.
- Yang, C., Guo, R., Jie, F., Nettleton, D., Peng, J., Carr, T., Yeakley, J.M., Fan, J. and Whitham, S.A. (2007) Spatial analysis of *Arabidopsis thaliana* gene expression in response to turnip mosaic virus infection. *MPMI*, **20**, 358–370.
- Yoshioka, H., Numata, N., Nakajima, K., Katou, S., Kawakita, K., Rowland, O., Jones, J.D.G. and Doke, N. (2003) *Nicotiana benthamiana* gp91 phox homologs NbrbohA and NbrbohB participate in H<sub>2</sub>O<sub>2</sub> accumulation and resistance to *Phytophthora infestans*. *Plant Cell*, **15**, 706–718. <https://doi.org/10.1105/tpc.008680.a>.
- Yu, H., Xiao, A., Dong, R. *et al.* (2018) Suppression of innate immunity mediated by the CDPK-Rboh complex is required for rhizobial colonization in *Medicago truncatula* nodules. *New Phytol.* **220**, 425–434. <https://doi.org/10.1111/nph.15410>.
- Zhou, J.M. and Zhang, Y. (2020) Plant immunity: danger perception and signaling. *Cell*, **181**, 978–989. <https://doi.org/10.1016/j.cell.2020.04.028>.
- Zielińska, L., Trzmiel, K. and Jeżewska, A. (2012) Ultrastructural changes in maize leaf cells infected with maize dwarf mosaic virus and sugarcane mosaic virus. *Acta Biol. Cracoviensia Ser. Bot.* **54**, 97–104. <https://doi.org/10.2478/v10182-012-0010-2>.
- Zurbriggen, M.D., Carrillo, N. and Hajirezaei, M.-R. (2010) ROS signalling in the hypersensitive response. *Plant Signal. Behav.* **5**, 393–396.